


First-order and continuous melting transitions in two-dimensional Lennard-Jones systems and repulsive disks

Amir Hajibabaei and Kwang S. Kim*

*Center for Superfunctional Materials, Department of Chemistry and Department of Physics,
Ulsan National Institute of Science and Technology (UNIST), Ulsan 44919, Korea*

 (Received 23 October 2017; revised manuscript received 11 December 2018; published 28 February 2019)

In two-dimensional Lennard-Jones (LJ) systems, a small interval of melting-mode switching occurs below which the melting occurs by first-order phase transitions in lieu of the melting scenario proposed by Kosterlitz, Thouless, Halperin, Nelson, and Young (KTHNY). The extrapolated upper bound for phase coexistence is at density $\rho \sim 0.893$ and temperature $T \sim 1.1$, both in reduced LJ units. The two-stage KTHNY scenario is restored at higher temperatures, and the isothermal melting scenario is universal. The solid-hexatic and hexatic-liquid transitions in KTHNY theory, even so continuous, are distinct from typical continuous phase transitions in that instead of scale-free fluctuations, they are characterized by unbinding of topological defects, resulting in a special form of divergence of the correlation length: $\xi \approx \exp(b|T - T_c|^{-\nu})$. Here such a divergence is firmly established for a two-dimensional melting phenomenon, providing a conclusive proof of the KTHNY melting. We explicitly confirm that this high-temperature melting behavior of the LJ system is consistent with the melting behavior of the r^{-12} potential and that melting of the r^{-n} potential is KTHNY-like for $n \leq 12$ but melting of the r^{-64} potential is first order; similar to hard disks. Therefore we suggest that the melting scenario of these repulsive potentials becomes hard-disk-like for an exponent in the range $12 < n < 64$.

DOI: [10.1103/PhysRevE.99.022145](https://doi.org/10.1103/PhysRevE.99.022145)

I. INTRODUCTION

Since the work of Mermin and Wagner, melting in two dimensions (2D) has been controversial [1,2]. Only quasi-long-range (QLR) positional order is possible in 2D; however, the orientational correlations could be long ranged. Kosterlitz, Thouless, Halperin, Nelson, and Young (KTHNY) theory proposes an upper bound for this phase of matter which is reached by unbinding of dislocations [3–6]. Beyond this threshold, the positional correlations are short ranged but the orientational correlations are quasi-long-ranged. This phase of matter intermediating between the solid and liquid phases is called hexatic. Unbinding of disclinations, which are another type of topological defects, destroys the QLR orientational order.

Typical continuous phase transitions occur between phases with long-ranged and short-ranged order. The spatial correlations of the order parameter in these phases have the form $c(r) \propto \exp(-r/\xi) + c(\infty)$, where $c(\infty)$ is nonzero (zero) for long (short)-ranged order, r is distance, and ξ is the correlation length. The correlations are algebraic at the critical point of these phase transitions: $c(r) \propto r^{-\eta}$, where the exponent η depends only on the basic characteristics such as dimensionality and symmetry properties of system. Thus, fluctuations of the order parameter do not have a length scale, and the thermodynamic properties of the system become independent of microscopic details; this is the source of universality in continuous phase transitions. In the vicinity of the critical temperature $T \rightarrow T_c$, this universality manifests itself in the exponents

of power-law divergence or vanishing of several quantities such as the correlation length $\xi \propto |T - T_c|^{-\nu}$, where ν is a universal number.

The defect-mediated continuous phase transitions proposed by Kosterlitz and Thouless (KT) occur between a phase in which the correlations are already algebraic and a phase with short-ranged correlations. Near liquid-hexatic phase transitions, KTHNY theory predicts that the correlation length of sixfold orientational order diverges as $\xi_6 \approx \exp(b/|T - T_c|^\nu)$, where ν equals 1/2 and b is a constant. A similar divergence with $\nu \approx 0.37$ is predicted for the positional correlation length near the hexatic-solid transition. KT theory has been controversial in the melting problem because it could be preempted by other mechanisms. For instance, Chui [7] proposed formation of grain boundaries which cause a first-order phase transition. The melting may also be induced by local disorder and phase coexistence [8]. The two phases in equilibrium are separated by an interface, and the free energy of the system is minimized when the interfacial area is minimized. Hence, the free energy barrier between two phases is proportional to the size of interface and the perimeter of the system rather than its volume.

Several scenarios have been observed experimentally: KTHNY melting for superparamagnetic colloids [9] and grain boundary melting for complex plasmas [10]. A liquid-hexatic phase coexistence was reported for colloids [11,12]. In simulation of hard disks, the hexatic-liquid phase transition was found to be first order [13,14] which is verified by experiment [15]. The range of pure hexatic phase was so narrow that by addition of a low concentration of smaller disks it totally disappeared [16]. By increasing the particle size polydispersity

*kimks@unist.ac.kr

of the hard disks the melting scenario switches to KTHNY transitions [17]. Hard regular polygons with seven or greater vertices melt similarly to the hard disks, while for polygons less than seven vertices melting depends on the shape and symmetry of the polygons [18]. For systems with $\propto r^{-n}$ repulsive interactions [19], a crossover occurs from KTHNY-like for $n \leq 6$ to hard-disk-like for $n > 6$. A similar crossover occurs for the Morse potential [20]. In simulations of other typical models of purely repulsive soft-core disks, the melting scenario changes from first order to continuous transitions as the density increases [21]. Switching of the melting scenario has also been confirmed in stiff and soft polymeric particles [22].

A variety of observed scenarios, which are mostly limited to purely repulsive soft and hard disks, show that melting in 2D is a complex phenomenon. Here we investigate melting of Lennard-Jones (LJ)-type systems in 2D. The potential is given by

$$U(r) = \begin{cases} 4\epsilon[(\sigma/r)^{12} - (\sigma/r)^6] - U_0 & r \leq r_c \\ 0 & r > r_c \end{cases}, \quad (1)$$

where $r_c = 2.5\sigma$ and U_0 is calculated by $U(r_c) = 0$. All quantities are expressed in LJ units with $\epsilon/\sigma/k_B = 1$. Also, the mass of an atom is 1 so that we may use “density” and “number density” interchangeably.

We explore the phase diagram of this model by extensive Monte Carlo simulations in a NVT ensemble. Isotherms spanning the melting phase transitions are simulated at several temperatures in the range $[0.5, 10]$, and finite-size effects are explicitly taken into account. We see that the melting scenario changes from first order to continuous phase transitions as the temperature becomes larger than $T \sim 1.1$. The two-step continuous melting scenario persists at high temperatures, at least up to the highest temperature we have checked. This seems to be at odds with a previous study [19] which suggests melting of power-law r^{-n} repulsive potentials is first order for $n > 6$. The LJ system may effectively be considered as power law with $n = 12$ at high temperatures. We address this by repeating Monte Carlo simulations for r^{-12} and r^{-64} potentials with a larger number of particles than considered before, and we show that for large enough systems, the first-order characteristics of melting of the r^{-12} potential reported in Ref. [19] disappear. Simulations with 512^2 particles are consistent with the continuous melting scenario that we observe for the LJ system at high temperatures.

II. METHOD

The event chain Monte Carlo (ECMC) algorithm [23,24] is used for the equilibration and sampling. A perfect hexagonal solid with the geometry of $(1, \sqrt{3}/2)La_0$ was considered as the initial state where $L = \sqrt{N}$ is the linear size of the system and a_0 is the natural lattice spacing for a given density ($\rho = 1/v$, $v = a_0^2 \sin(\pi/3)/2$). Simulations were carried out in the NVT ensemble subject to the periodic boundary conditions. We considered nine isotherms at temperatures $T = 0.5, 0.7, 1, 1.5, 2, 3, 5, 7, \text{ and } 10$, about 25 densities with spacing of $\delta\rho \sim 0.002$ for each isotherm, and three sizes of $N = 128^2, 256^2, 512^2$ particles.

The ECMC algorithm is a rejection-free Monte Carlo method that displaces a chain of particles in one move. To ensure equilibration of systems as large as 512^2 particles, $(1 - 2) \times 10^7$ displacements per particle were performed. This length for the simulations is chosen so that two simulations with different initial configurations converge. The equilibration is discussed with more details in the Supplemental Material [25] (SM).

III. PHASE DIAGRAM

The phase diagram of this system obtained from ECMC simulations is shown in Fig. 1(a). Detailed plots of equations of state and relevant correlation functions are in the SM [25]. When $T \leq 1.0$, there is a Mayer-Wood loop [26] in the equation of state, indicating a phase coexistence. Then the equilibrium pressure p_0 and the volume interval $\Delta v = v_l - v_s$ of phase coexistence are determined by Maxwell constructions. The free energy barrier ΔF is related to the integral of the equation of state in this interval. ΔF should be proportional to the linear size of system ($\propto \sqrt{N}$) at phase coexistence and $\Delta f = \Delta F/N \propto 1/\sqrt{N}$. This is asymptotically true at $T = 0.5$ [Fig. 1(c)]. By extrapolation, the phase coexistence interval disappears at $T \approx 1.1$ [Fig. 1(d)].

Here we introduce a simple transformation so that the regions in the phase diagram are easily referenced. The order-disorder curve (obtained by fitting) is defined by

$$\rho_0(T) = a(\ln(T))^2 + b\ln(T) + c \quad T \in [0.5, 10], \quad (2)$$

with the fit parameters $a = 0.0183$, $b = 0.0973$, and $c = 0.8839$. This is shown by the solid green+black (light+dark gray) curve in the phase diagram of Fig. 1(a). On this curve the orientational correlations change from QLR to short ranged corresponding to the hexatic-to-liquid phase transition. If the hexatic phase is preempted by phase coexistence, this curve is the density at which the two coexisting phases occupy equal volumes in the system. We define the “relative density” as

$$\Delta\rho(T) = \rho - \rho_0(T), \quad (3)$$

and $(\Delta\rho(T), T)$ are hereafter considered as the independent parameters instead of (ρ, T) . In this notation the extrapolated liquid-hexatic-coexistence triple point in the phase diagram Fig. 1(a) is located at $(\Delta\rho, T) \approx (0, 1.1)$.

The solid-hexatic and hexatic-liquid phase transitions at high temperatures are driven by the (QLR to short ranged) transformations of the positional and orientational correlations, which are discussed next.

IV. CORRELATIONS

The hexagonal order parameter (hex-order) is defined as

$$\psi_i = \frac{1}{n_i} \sum_j (A_{ij}/A_i) e^{6i\theta_{ij}}, \quad (4)$$

where the sum is over the nearest neighbors of i ; n_i is the number of nearest neighbors; θ_{ij} is the angle of $\vec{r}_j - \vec{r}_i$ with respect to the x axis; A_{ij} is the length of the edge that the Voronoi polygons of particles i and j share; and $A_i = \sum_j A_{ij}$. Clearly, the neighborhood relations are weighted [27]. Another common definition of the hex-order is $\psi_i = (1/6) \sum_{j=1}^6 e^{6i\theta_{ij}}$,

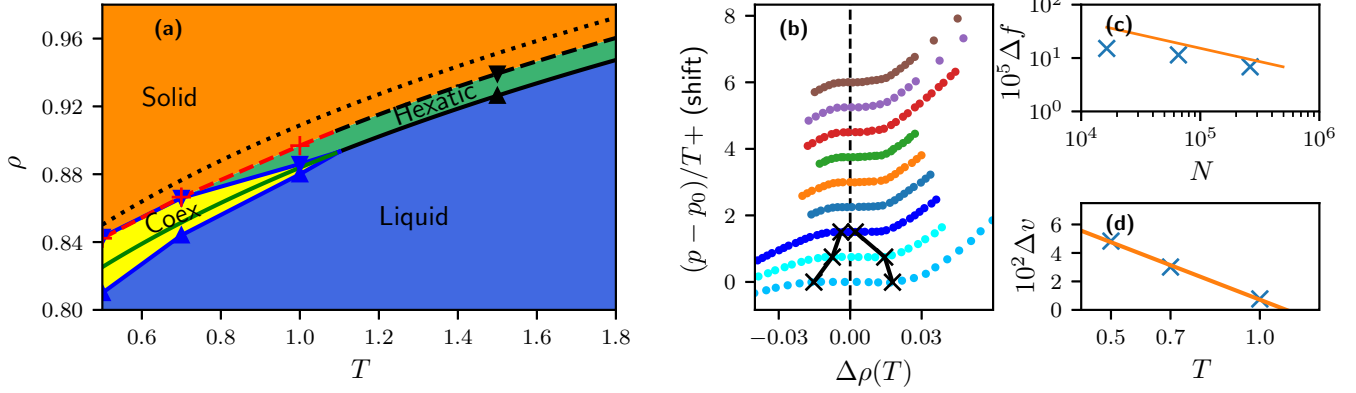


FIG. 1. (a) Phase diagram of the LJ system for 512^2 particles (lines are interpolations). Continuation of the hexatic phase with similar density width is verified up to $T = 10$. The extrapolated upper bound for phase coexistence is at $\rho \sim 0.893$ and $T \sim 1.1$. The green+black (light+dark gray) solid curve is $\rho_0(T)$ given by Eq. (2). Above the red+black (light+dark gray) dashed curve orientational correlations are long ranged. Above the dotted curve, positional correlation functions are perfectly power law [$g(x, 0) \propto x^{-\eta}$] with an exponent $\eta \leq 1/3$. Between the dashed and dotted curves $g(x, 0)$ decays as a power law up to moderate distances (with η slightly higher than $1/3$) but slightly faster than power law at the largest distances due to the finite-size effects. The uncertainty in density is 0.005 for the dotted line and 0.002 for all other lines and symbols. (b) The shifted pressure-density equations of states at temperatures, from bottom to top, are 0.5, 0.7, 1, 1.5, 2, 3, 5, 7, and 10 for 512^2 particles. Boundaries of phase coexistence are obtained by Maxwell constructions and marked by \times signs on isotherms [and by blue triangles in (a)]. (c) Scaling of the free energy barrier per particle with the system size at $T = 0.5$. The solid line is proportional to $1/\sqrt{N}$. (d) The volume ($v = 1/\rho$) interval of phase coexistence disappears at $T \sim 1.1$.

where the sum is over six closest neighbors. In the following we distinguish between two definitions by using the terms weighted and weightless hex-order. The weighted definition is computationally much more expensive, but it has the benefit of being a continuous function. We have used this definition in all of our ECMC simulations. The orientational order parameter is $\Psi = 1/N \sum_i \psi_i$, and the orientational correlation function is

$$g_6(r) = \left\langle \frac{1}{N} \sum_{i,j} \psi_i \psi_j^* \delta(r - |\vec{r}_i - \vec{r}_j|) \right\rangle. \quad (5)$$

The 2D pair distribution function is

$$g(x, y) = \frac{1}{\rho} \left\langle \frac{1}{N} \sum_i \rho(x - x_i, y - y_i) \right\rangle, \quad (6)$$

where $\rho(\vec{r}) = \sum_j \delta(\vec{r} - \vec{r}_j)$, and the direction of the x axis is parallel to the direction of symmetry axis of solid. By integrating and normalizing this function at constant radius, $x^2 + y^2 = r^2$, the conventional radial distribution function (RDF) $g_r(r)$ is recovered.

The spatial form of these correlation functions at important temperatures and densities are plotted in the SM [25]. We extract the main information from these correlation functions by fitting them to the exponential $\propto \exp(-r/\xi)$ and algebraic $\propto r^{-\eta}$ forms. The temperature and density dependence of the correlation length ξ and/or the exponent η provides an abstract description of the correlation functions.

In the liquid phase, the orientational correlations $g_6(r)$ are short ranged and described by a correlation length ξ_6 . These correlations become algebraic in the hexatic phase and are described by an exponent η_6 . $\xi_6(\Delta\rho, T)$ and $\eta_6(\Delta\rho, T)$ are plotted in Figs. 2(a) and 2(b). They become independent of temperature at $T > 1.1$. The solid curve (fit to bullets) in

Fig. 2(a) is a fit to the correlation length with the form

$$\xi_6(\Delta\rho) = \exp(b/\sqrt{\alpha_N - \Delta\rho}), \quad (7)$$

where b equals 0.28 and the size dependence of correlation length is expressed in α_N , which is equal to 0.0027, 0.0016, and 0.0007 for the sizes of 128^2 , 256^2 , and 512^2 particles (see Fig. S5 [25] for size dependence of ξ_6). From these numbers, it is easy to see that $\alpha_N \propto 1/\sqrt{N}$. This form of divergence of correlation length strongly supports KTHNY theory, while the slower variation observed at low temperatures is consistent with phase coexistence.

The exponent η_6 is $\sim 1/4$ when $\Delta\rho = 0$ and it becomes zero at $(\Delta\rho, T) \approx (0.013, T > 1.1)$, $(0.015, 0.7)$, and $(0.017, 0.5)$ [see inset of Fig. 2(b)]. The orientational correlations are long ranged beyond these densities. In Fig. 1(a), $\Delta\rho(T) = 0.013$ is plotted in the black (dark gray) dashed curve, while the nonuniversal values at $T < 1.1$ are plotted in the red (light gray) dashed curve. At $T > 1.1$, even so g_6 becomes perfectly long ranged at $\Delta\rho = 0.013$, $g(x, 0)$ and g_r become perfectly power law at 0.025 ± 0.005 (shown by the dotted curve). The true solid-hexatic phase transition should be at a density in this range. Within this range the positional correlations decay faster than a power law at distances larger than $r \sim \zeta/2$, where $\zeta = L/2$ is the largest distance in the system, but are perfectly power law at shorter distances and, overall, are better described with a power law than an exponential function [Fig. 2(c)].

For an infinite system there are clear distinctions between short-ranged, long-ranged, and power-law correlations. In such a system the respective transformations in g_6 and $g(x, 0)$ near solid-hexatic transition should occur at the same density. But for a finite system, there could be a range of functions between clear short-ranged and clear power-law limits. For

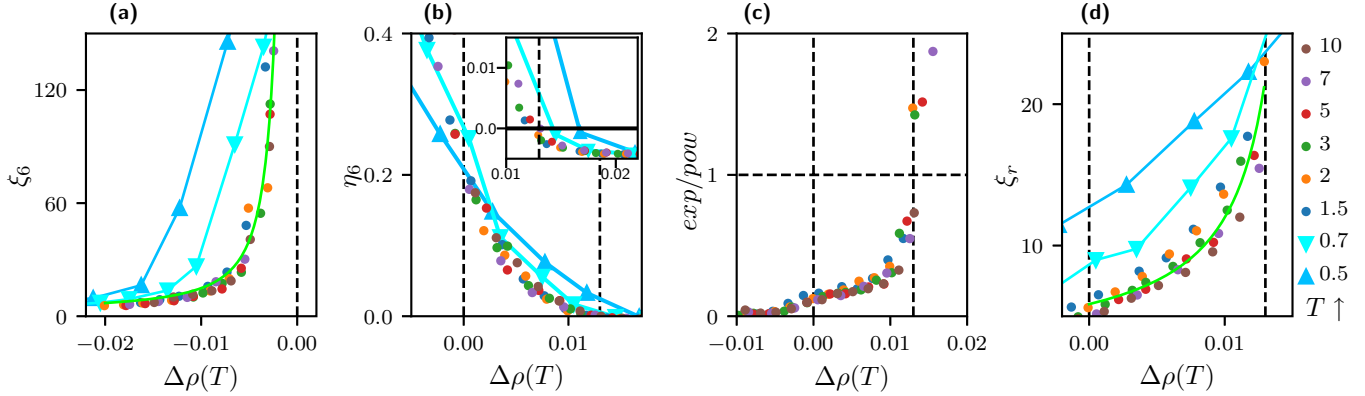


FIG. 2. Temperature dependence of correlation-derived quantities for 512^2 particles. Plots of raw correlation functions and size dependence analysis are provided in the SM [25]. The color codes for temperatures are given at the right side. The scatter plots verify that, for instance, $\xi_6(\Delta\rho, T) \rightarrow \xi_6(\Delta\rho)$ at $T > 1.1$. The correlations at $T = 1$ differ only slightly from that of $T > 1.1$. (a) Orientational correlation length. (b) Exponent of the algebraic fits to the orientational correlations. (c) Relative error of exponential and power-law fits to the RDF. Error is estimated from variance of the difference between the fit and the raw correlation function at $r > 10$. (d) Correlation length of the RDF.

instance, a function could decay faster than a power law but still be nonzero at the largest meaningful distance.

In simulation of hard disks [13], g_6 became perfectly long ranged immediately above the phase coexistence but $g(x, 0)$ was still “clearly short ranged.” Since long-ranged orientational correlations are inconsistent with short-ranged positional correlations, they concluded that the system must be in hexatic phase with a power law g_6 but with a very small exponent $\eta_6 \rightarrow 0^+$. Here, up to the largest systems simulated, the positional correlations are not “clearly short ranged” beyond $\Delta\rho > 0.013$. Thus we perform a finite-size scaling analysis and exploit the universality of correlations at $T > 1.1$. The $\Delta\rho$ at which η_6 becomes zero increases slowly with the system size (see Fig. S5 [25]): 0.010 for 128^2 , 0.012 for 256^2 , and 0.013 for 512^2 particles, hence very close to 0.013 for larger sizes.

The correlation length ξ_r of the RDF, plotted in Fig. 2(d), has very little temperature dependence. The solid curve (fit to

bullets) is obtained by fitting ξ_r to

$$\xi_r(\Delta\rho') = \exp(c/|\beta_N - \Delta\rho'|^\nu), \quad (8)$$

where $\Delta\rho'(T) = \Delta\rho(T) - 0.013$, $\nu = 0.39$, $c = 0.375$, and $\beta_N = 0.007, 0.005, 0.004$ for the sizes $128^2, 256^2, 512^2$. Especially near $\Delta\rho(T) = 0.013$ the temperature dependence of ξ_r is much weaker than its size dependence. If the exponential form is assumed for g_r at $\Delta\rho > 0.013$, the resulting correlation length shows a size dependence which switches its behavior at 0.013 (see Fig. S5(d) [25]). Therefore the density at which η_6 becomes zero yields a coherent picture for the solid-hexatic phase transition.

In summary, we suggest that vanishing of η_6 accompanied by finite-size scaling should be used for determination of the hexatic-solid phase transition. Based on this criterion, the dashed lines in the phase diagram Fig. 1(a) are very close to the upper bounds of the hexatic phase in thermodynamic limit and the hexatic phase totally disappears at $0.7 < T < 1$.

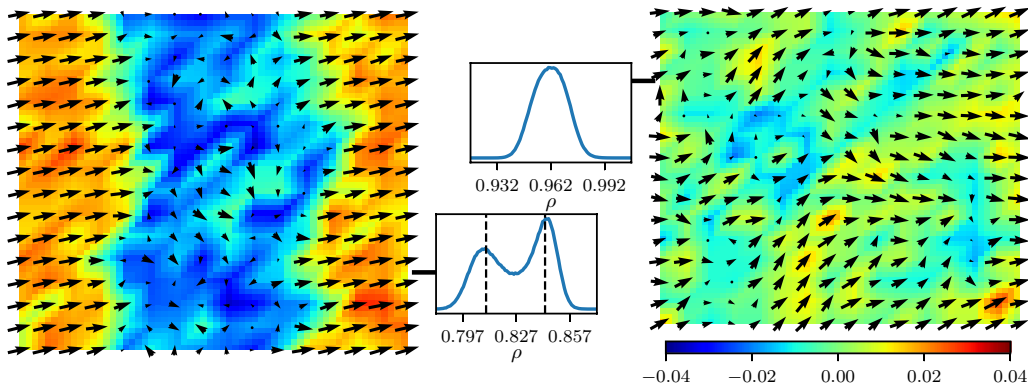


FIG. 3. Solid-liquid phase coexistence vs hexatic phase. Both systems are at relative density $\Delta\rho = 0.002$ with 512^2 particles but at different temperatures: 0.5 (left) and 2 (right). This snapshot is reached after 3×10^8 MD steps. The systems are divided into 16×16 subsystems to analyze the fluctuations. The color-bar indicates $\rho(r) - \bar{\rho}$, and the histograms show the probability distribution function (PDF) of density in subsystems obtained from ensemble averaging. The dashed lines coinciding with the two maxima of PDF, on the left histogram, are the lower and upper densities for solid-liquid coexistence obtained from ECMC simulations. The vectors on top of the color maps show the local orientational order: $(\text{Re}(\Psi), \text{Im}(\Psi))$. In coexistence the orientation is uniform in the solid portion of system, while in hexatic phase there are mobile topological defects in the orientational field (see movies in SM [25]).

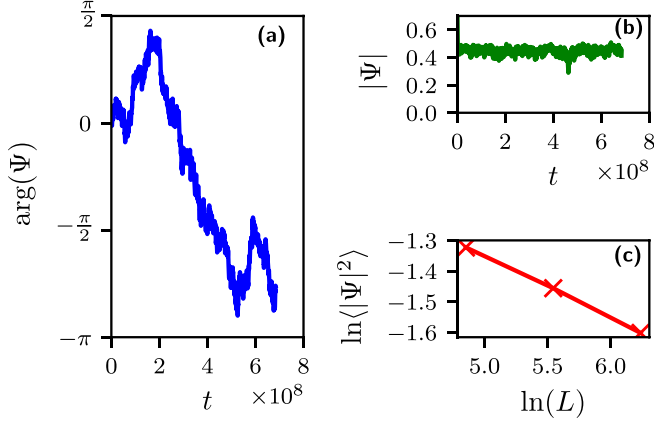


FIG. 4. Orientational order in hexatic phase. (a, b) Dynamics of orientational order parameter $\Psi = |\Psi|e^{i\arg(\Psi)}$ with time step 0.001, at relative density $\Delta\rho = 0.002$, at $T = 2$, and for 512^2 particles. t is number of MD steps. (c) Finite-size scaling of spontaneous orientational order. $L = 128, 256, 512$ is the linear size of system.

V. MOLECULAR DYNAMICS STUDY

To verify some of these findings with another independent method, we performed targeted molecular dynamics simulations using LAMMPS [28] for the potential given by Eq. (1). These simulations are limited to $\Delta\rho(T) = 0.002$ (just above the order-disorder line) at $T = 0.5, 2, 3$, and 10 with a time step of 0.001. According to the ECMC simulations, this $\Delta\rho$ falls into the coexistence interval at $T = 0.5$ while the hexatic phase is expected at other temperatures. A snapshot of spatial fluctuations of density and orientational order is shown in Fig. 3, where the weightless definition of hex-order is used in this case. The histogram of density fluctuations has a single peak at $T = 2$, while it has two distinct peaks at $T = 0.5$. These two peaks coincide with the lower and upper densities of phase coexistence obtained from the ECMC simulations. In addition, the snapshot shows that regions of low and high density tend to separate and create an interface.

The dynamics of orientational order parameter with time, at $T = 2$, is shown in Fig. 4. In the hexatic phase, a finite system has nonvanishing spontaneous orientational order ($|\Psi| > 0$), but the angle of orientation changes with time in a

manner similar to a random walk. This results in vanishing of the time average of order parameter $\int_0^\infty \Psi(t)dt \rightarrow 0$ where, from Fig. 4(c), the spontaneous order vanishes only when the size of system is infinity: $\langle |\Psi|^2 \rangle \propto L^{-\eta_6}$ with $\eta_6 = 0.20$. Similar analysis at $T = 3$ and 10 results in $\eta_6 = 0.21$ and 0.19, respectively. The results of the MD simulations at $T = 10$ are presented in more detail in the SM [25] (see Fig. S14).

VI. REPULSIVE DISKS REVISITED

It is suggested that melting of soft disks interacting by a repulsive $\propto r^{-n}$ potential is first order when $n > 6$ [19]. The Lennard-Jones potential may effectively be considered as $\propto r^{-12}$ potential at high enough temperatures. Here we showed that melting of the Lennard-Jones system is continuous at high temperatures. There is an apparent controversy here which we will address in the following.

In Ref. [19], the equations of states were calculated for systems with $\sim 256^2$ particles. Our simulations of the Lennard-Jones system at $T = 10$ with the same size also shows an S loop in the equation of state, but this loop disappears for larger systems with 512^2 particles. Therefore finite-size scaling appears to be a critical issue here.

Here we repeat Monte Carlo simulations for the potential defined by

$$U(r) = \begin{cases} \epsilon(\sigma/r)^n - U_0 & r \leq r_c \\ 0 & r > r_c \end{cases}, \quad (9)$$

where $r_c = 1.8\sigma$ (same cutoff used in Ref. [19]) and U_0 is calculated by $U(r_c) = 0$. The units are chosen where $\sigma, \epsilon = 1$ and simulations are done for $n = 12, 64$ cases at unit temperature. The weightless definition of hex-order is applied in these simulations. We chose the Metropolis algorithm because of more trivial parallelization for lengthy simulations. Equations of states are calculated for $N = 128^2, 256^2$, and 512^2 particles. Simulations for $N = 1024^2$ particles are carried out only at critical densities of 1.002 for $n = 12$ and 0.894 for $n = 64$. About 8×10^7 Monte Carlo sweeps are performed in most cases.

The S loop in the pressure-density equation of state of the r^{-12} potential disappears for 512^2 particles [Fig. 5(a)]. The power-law finite-size scaling of the orientational order parameter at $\rho = 1.002$ [Fig. 5(b)] is an important

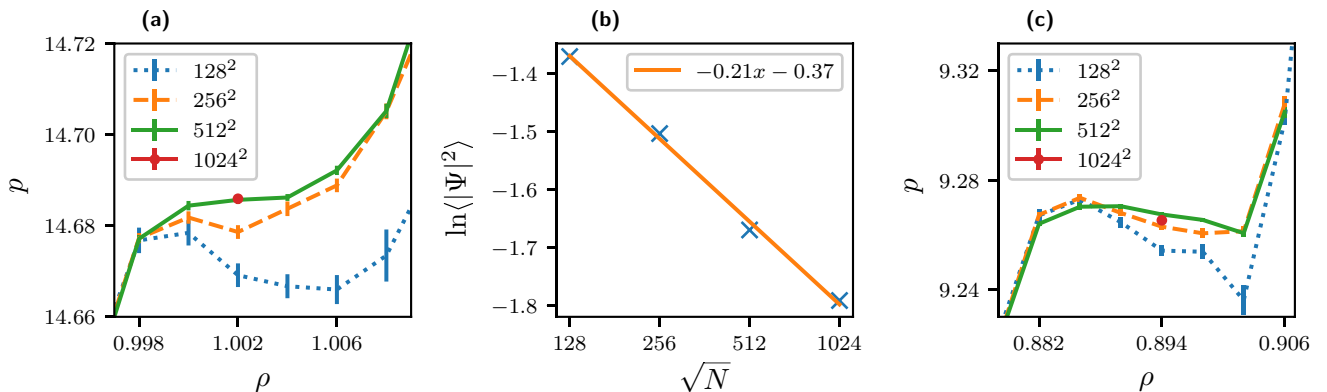


FIG. 5. Pressure-density equations of state for (a) r^{-12} and (c) r^{-64} potentials. (b) Power-law finite-size scaling of the bond orientational order at $\rho = 1.002$ for r^{-12} potential. Notice the logarithmic scale of the horizontal axis in (b) and that $x = \ln\sqrt{N}$ in the legend.

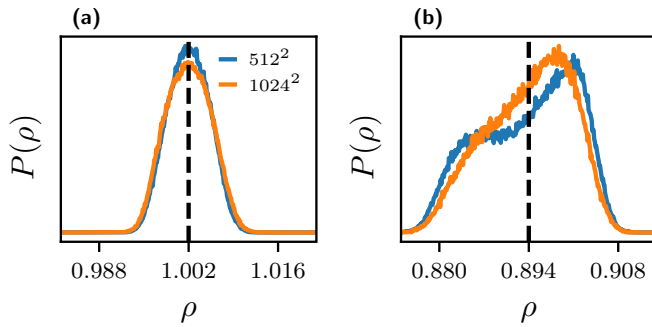


FIG. 6. Fluctuations of local density when the global density is fixed at (a) $\bar{\rho} = 1.002$ for the r^{-12} and (b) $\bar{\rho} = 0.894$ for the r^{-64} potentials.

characteristic of the continuous phase transitions. In addition, we have checked for the homogeneity of system by sampling the local density distribution. The local density is defined as the number density of a block of the size $\sim 100\sigma \times 100\sigma$. Such a block is chosen randomly within the system in every sampling. A histogram of these local densities is shown in Fig. 6. This figure shows that melting of the r^{-12} potential occurs through homogeneous systems while melting of the r^{-64} occurs through hexatic-liquid mixtures.

Thus melting of the r^{-12} potential has all of the characteristics of the continuous phase transitions, and the S loops in the equations of states of smaller systems ($N \leq 256^2$) are only due to the finite-size effects. Melting of the r^{-64} potential is first order, similar to the hard disks [13]. The crossover from KTHNY-like to hard-disk-like melting of the repulsive disks with $\propto r^{-n}$ potential occurs for an exponent in the range $12 < n < 64$.

VII. CONCLUSION

To summarize, we showed that the KTHNY melting scenario is preempted by phase coexistence at $T < 1.1$ in the

Lennard-Jones system. This occurs because the energy of local vacancy aggregates becomes vanishingly small in this part of the phase diagram [29,30]. At higher temperatures the melting scenario is consistent with KTHNY theory. The KTHNY theory is derived by the assumption of harmonic interactions. Since the anharmonic effects are weaker in denser LJ systems [29,30], the KTHNY theory is accurate at high temperatures where melting occurs at higher densities.

We also revisited melting of the $\propto r^{-n}$ potential for two special cases of $n = 12$ and 64 by simulating larger systems than before. It is concluded that melting of the $n = 12$ case is continuous in the thermodynamic limit, consistent with the melting scenario we observe for the LJ system at high temperatures. Therefore we suggest that the critical exponent for the KTHNY to first-order crossover in the melting scenario of these systems should be a number in the range $12 < n < 64$ instead of $n \sim 6$, as suggested in Ref. [19].

Thus, in addition to having a harder repulsive potential, introducing an attractive well is another route towards first-order melting. The difference is that in the former melting is derived by entropic terms, while in the latter energetics are important. That is, due to the competition of lattice constant and length scale of the attractive well, vacancies may or may not be favorable. For instance, if a cavity is created within the solid it may be stable if attractive forces are present, but it is certainly unstable if the forces are purely repulsive.

ACKNOWLEDGMENTS

This work was supported by the NRF (National Honor Scientist Program, Grant No. 2010-0020414) and KISTI (Grants No. KSC-2015-C3-002, No. KSC-2016-C3-0074, and No. KSC-2017-C3-0081).

-
- [1] N. D. Mermin and H. Wagner, *Phys. Rev. Lett.* **17**, 1133 (1966).
 - [2] N. D. Mermin, *Phys. Rev.* **176**, 250 (1968).
 - [3] J. M. Kosterlitz and D. J. Thouless, *J. Phys. C* **6**, 1181 (1973).
 - [4] B. I. Halperin and D. R. Nelson, *Phys. Rev. Lett.* **41**, 121 (1978).
 - [5] D. R. Nelson and B. I. Halperin, *Phys. Rev. B* **19**, 2457 (1979).
 - [6] A. P. Young, *Phys. Rev. B* **19**, 1855 (1979).
 - [7] S. T. Chui, *Phys. Rev. Lett.* **48**, 933 (1982).
 - [8] E. Domany, M. Schick, and R. H. Swendsen, *Phys. Rev. Lett.* **52**, 1535 (1984).
 - [9] K. Zahn, R. Lenke, and G. Maret, *Phys. Rev. Lett.* **82**, 2721 (1999).
 - [10] V. Nosenko, S. K. Zhdanov, A. V. Ivlev, C. A. Knapek, and G. E. Morfill, *Phys. Rev. Lett.* **103**, 015001 (2009).
 - [11] A. H. Marcus and S. A. Rice, *Phys. Rev. Lett.* **77**, 2577 (1996).
 - [12] B. Lin and L. Chen, *J. Chem. Phys.* **126**, 034706 (2007).
 - [13] E. P. Bernard and W. Krauth, *Phys. Rev. Lett.* **107**, 155704 (2011).
 - [14] M. Engel, J. A. Anderson, S. C. Glotzer, M. Isobe, E. P. Bernard, and W. Krauth, *Phys. Rev. E* **87**, 042134 (2013).
 - [15] A. L. Thorneywork, J. L. Abbott, D. G. A. L. Aarts, and R. P. A. Dullens, *Phys. Rev. Lett.* **118**, 158001 (2017).
 - [16] J. Russo and N. B. Wilding, *Phys. Rev. Lett.* **119**, 115702 (2017).
 - [17] P. S. Ruiz, Q. Lei, and R. Ni, [arXiv:1804.05582](https://arxiv.org/abs/1804.05582).
 - [18] J. A. Anderson, J. Antonaglia, J. A. Millan, M. Engel, and S. C. Glotzer, *Phys. Rev. X* **7**, 021001 (2017).
 - [19] S. C. Kapfer and W. Krauth, *Phys. Rev. Lett.* **114**, 035702 (2015).
 - [20] S. I. Lee and S. J. Lee, *Phys. Rev. E* **78**, 041504 (2008).
 - [21] M. Zu, J. Liu, H. Tong, and N. Xu, *Phys. Rev. Lett.* **117**, 085702 (2016).
 - [22] Y. Li and M. P. Ciamarra, *Phys. Rev. Mater.* **2**, 045602 (2018).
 - [23] E. P. Bernard, W. Krauth, and D. B. Wilson, *Phys. Rev. E* **80**, 056704 (2009).

- [24] M. Michel, S. C. Kapfer, and W. Krauth, *J. Chem. Phys.* **140**, 054116 (2014).
- [25] See Supplemental Material at <http://link.aps.org/supplemental/10.1103/PhysRevE.99.022145> for details of equilibration by ECMC algorithm and analysis, visualizations, and finite size scaling of the correlation functions.
- [26] J. E. Mayer and W. W. Wood, *J. Chem. Phys.* **42**, 4268 (1965).
- [27] W. Mickel, S. C. Kapfer, G. E. Schröder-Turk, and K. Mecke, *J. Chem. Phys.* **138**, 044501 (2013).
- [28] S. Plimpton, *J. Comput. Phys.* **117**, 1 (1995).
- [29] B. Joos and M. S. Duesbery, *Phys. Rev. Lett.* **55**, 1997 (1985).
- [30] B. Joos and M. S. Duesbery, *Phys. Rev. B* **33**, 8632 (1986).